International Journal of Mechanical, Industrial and Aerospace Sciences
ISSN: 2517-9950
Vol:12, No:5, 2018

The Onset of Ironing during Casing Expansion

W. Assaad, D. Wilmink, H. R. Pasaribu, H. J. M. Geijselaers

***Abstract*—**Shell has developed a mono-diameter well concept for oil and gas wells as opposed to the traditional telescopic well design. A Mono-diameter well design allows well to have a single inner diameter from the surface all the way down to reservoir to increase production capacity, reduce material cost and reduce environmental footprint. This is achieved by expansion of liners (casing string) concerned using an expansion tool (e.g. a cone). Since the well is drilled in stages and liners are inserted to support the borehole, overlap sections between consecutive liners exist which should be expanded. At overlap, the previously inserted casing which can be expanded or unexpanded is called the host casing and the newly inserted casing is called the expandable casing. When the cone enters the overlap section, an expandable casing is expanded against a host casing, a cured cement layer and formation. In overlap expansion, ironing or lengthening may appear instead of shortening in the expandable casing when the pressure exerted by the host casing, cured cement layer and formation exceeds a certain limit. This pressure is related to cement strength, thickness of cement layer, host casing material mechanical properties, host casing thickness, formation type and formation strength. Ironing can cause implications that hinder the deployment of the technology. Therefore, the understanding of ironing becomes essential. A physical model is built in-house to calculate expansion forces, stresses, strains and post expansion casing dimensions under different conditions. In this study, only free casing and overlap expansion of two casings are addressed while the cement and formation will be incorporated in future study. Since the axial strain can be predicted by the physical model, the onset of ironing can be confirmed. In addition, this model helps in understanding ironing and the parameters influencing it. Finally, the physical model is validated with Finite Element (FE) simulations and small-scale experiments. The results of the study confirm that high pressure leads to ironing when the casing is expanded in tension mode.

***Keywords*—**Casing expansion, cement, formation, metal forming, plasticity, well design

I. Introduction

CASING strings are inserted in borehole to support it from collapse after drilling. A telescopic well is the conventional well design. Shell designed Mono-Diameter (MOD) wells as an alternative to the conventional telescopic well design. MOD wells have almost the same diameter from top to bottom of the well. MOD well is accomplished by casing expansion at downhole [1]-[3].

The expansion process is performed by a cone pulled by the drill string through the casing which is deformed plastically. A Top Anchor and Pull (TAaP) system is one of the systems that are used for the casing expansion. In this system, ironing may occur.

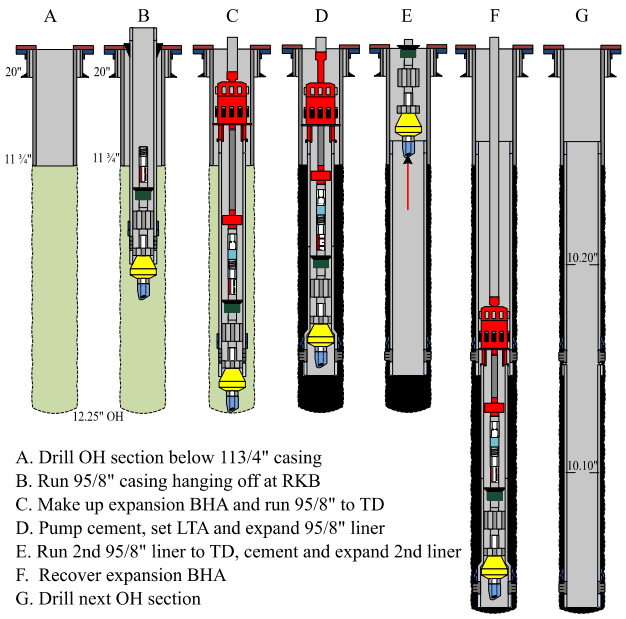

Fig. 1 MOD deployment process of TAap system

The MOD deployment process of the TAaP system is shown in Fig. 1 and described in the following sequence [1]:

1. The open hole section to deploy an expandable liner is drilled or under-reamed to a desired depth.
2. The expandable liner is made up to the desired deployed length and it is hung off at Rig Kelly Bushing (RKB).
3. Bottom Hole Assembly (BHA) is attached to the expandable liner with a special first casing joint. An inner drill pipe string is deployed through internal-diameter (ID) of the made-up liner and attached to the expansion BHA with the Liner Top Anchor (LTA). Then the liner is run to the Target Depth (TD).
4. At the target depth in the well the LTA is activated by hydraulic pressure which locks it to the host casing. Cement slurry is pumped and the expansion is initiated by pulling the cone utilizing rig draw works. During initial stage of expansion, an annular zonal seal is activated to prevent cement U-tubing. In addition, an Open Hole Anchor (OHA) which locks the bottom of the expanded liner to the formation. Continued rig drill pipe overpull

W. Assaad is with Shell Global Solutions International B.V., Kessler Park 1, 2288 GS Rijswijk, The Netherlands (corresponding author, phone: +31704473886; e-mail: Wissam.Assaad@shell.com).
D. Wilmink is with Nederlande Aardolie Maatschappij B. V. (NAM), Assen, 9405 TA, The Netherlands (e-mail: Daan.Wilmink@shell.com).
H. R. Pasaribu is with Shell Global Solutions International B.V., Kessler Park 1, 2288 GS Rijswijk, The Netherlands (e-mail: Henry.Pasaribu@shell.com).
H. J. M. Geijselaers is with Nonlinear Solid Mechanics, Department of Mechanics of Solids, Surfaces and Systems, University of Twente, Drienerlolaan 5, 7522NB, Enschede, The Netherlands (e-mail: h.j.m.geijselaers@ctw.utwente.nl).

expands the remaining part of the expandable liner. Once the cone is in the overlap section with the host casing, the LTA automatically releases enabling the cone to pop out by the end of overlap section and retrieval of the expansion BHA.

5. A second expandable liner is run to TD. A cement slurry is pumped and the liner is expanded.
6. Expansion BHA is recovered.
7. A next OH is drilled.

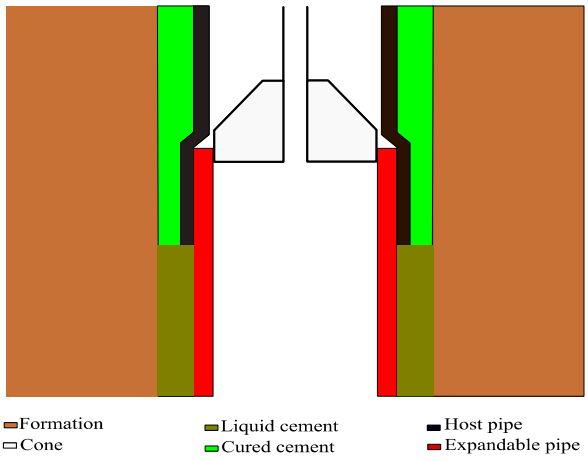

Fig. 2 Overlap expansion: expansion of expandable casing against host casing, cement and formation

When a casing is expanded, material flows mainly in circumferential direction to increase its diameter. After expansion, this leads to a decrease in both wall thickness and casing length. However, during overlap expansion, depicted in Fig. 2, a pressure is exerted on the outer surface of the expandable casing. This pressure is resulted from the resistance of the host casing, cured cement layer and formation. It contributes in decreasing wall thickness. If the wall thickness decreases below a certain limit, an increase in casing length starts occurring. This phenomenon is known as ironing; a metal forming process of wall thinning of a deep-drawn cylindrical cup which generates a product with a uniform thickness and longer length [4]-[7]. Since ironing occurs due to an external pressure on the outer surface of the casing, it can be called as hydrostatic ironing [7]. The ironing which takes place during casing expansion is unfavorable and it must be avoided because it has the following implications on the MoD deployment process:

1. Difficulty in releasing the LTA. In a vertical borehole, this tool can move freely downwards but not upwards. When the expandable casing starts to elongate, an additional force is exerted on the LTA from the top of the expandable casing. This force prevents it from being released.
2. Cone getting Stuck. During elongation, casing exerts a force on the LTA and compressive stresses are generated in the expandable casing. The compressive stresses cause thickening or buckling of the casing.
3. Generation of new surfaces with unknown lubrication quality which leads to an increase in expansion force which is limited by the pulling capacity of the rig or load carrying capacity of the drill string.

The paper describes the physical model developed in-house to calculate the expansion force and post expansion dimensions of the casing in free and overlap expansion. It is divided into: (1) Physical Modelling (2) Results (3) Conclusion.

II. Physical Modelling

A. Free Expansion

Free expansion denotes to a single casing expansion. This situation is like expansion of a single casing in MoD deployment process, where the cement layer is still in liquid state. The plastic deformation of the casing during expansion occurs in several stages such as bending outward, bending inward, diameter increase, bending inward and bending outward as illustrated in Fig. 3. Bending at first and last stages, occur at cone nose with a radius R_{nose} and cone roundoff with a radius R_{roff}. The inclination angle in middle of expansion process has referred to as α.

A one dimensional (1D) is built to calculate the expansion force along axial direction. The following assumptions are applied to the model:

1. Isotropic material behavior
2. Isotropic hardening
3. Incompressible material
4. Pure plastic deformation
5. Thin walled pressure vessel
6. Coulomb friction model

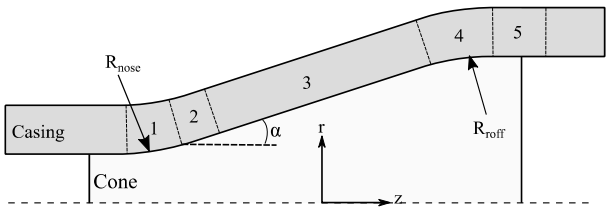

Fig. 3 Stages of plastic deformation of casing during expansion. A: cone, B: Expandable casing. (1) bending outward, (2) bending inward, (3) diameter increase (4) bending inward (5) bending outward

In this model, the expanding casing is discretized in longitudinal direction into equal parts. At each part the stress and strain state are calculated. An equivalent strain $d\varepsilon_e$ is calculated at each time step and therefore the stress state and hardening of the material are addressed. Since FE simulations show that the shear doesn't have a significant contribution to the internal work, the elements with their principal stresses rotate according to deformation zones as shown in Fig. 4. Since calculations of stresses and strains are most convenient in principal coordinate system, this coordinate system is used in the model as shown in Fig. 4. To avoid confusion with the global coordinate system, the notation σ_m, σ_θ and σ_r will be

used to indicate the meridional, circumferential and thickness (radial) stress respectively.

The differential equations of the stress state are determined by applying Newton's first law of motion in m and r directions. The forces applied on an element of casing during expansion are illustrated in Fig. 5. The entire derivation can be found in Appendix.

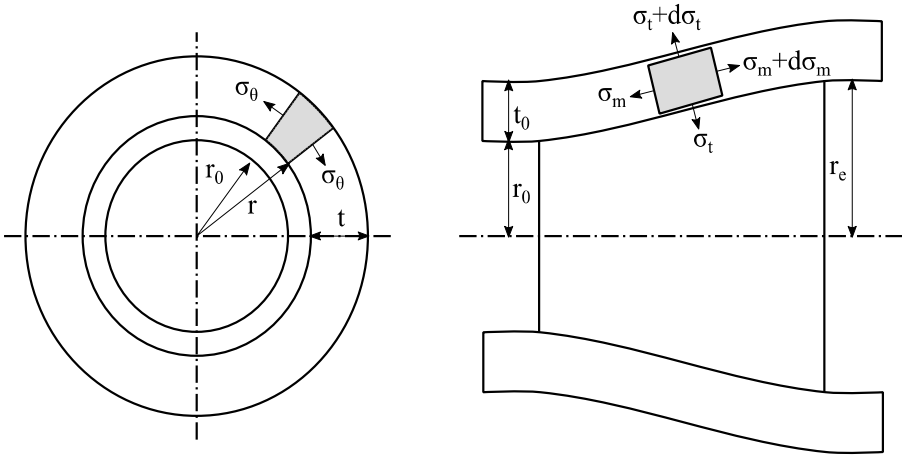

Fig. 4 Direction of the principal stresses during expansion

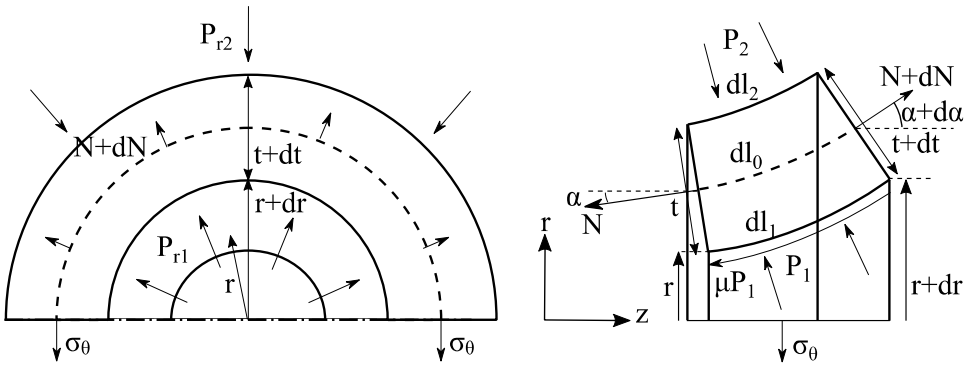

Fig. 5 Schematic overview acting on a slice of the expanding casing

B. Overlap Expansion

In overlap expansion, two casings in overlap are expanded simultaneously with the cone. The two casings including the inner and outer casings are called the expandable and host casing respectively as depicted in Fig. 6. The cone with defined dimensions expands the expandable casing. The expandable casing follows the cone profile to a certain level. However, the host casing is expanded with the expandable casing which can be represented as a virtual cone. Since the host casing is expanded with a low expansion ratio, the host casing will not fully follow the profile of the virtual cone. Therefore, the geometrical features of the virtual cone such as radii at nose and round off, and angle require to be determined. FE simulations show that geometrical features depend on dimension of host casing, expansion ratio and mechanical properties of host casing. The expansion force component required to expand the host casing is calculated in the same manner as the expansion force required to expand the expandable casing. The following assumptions are applied in calculation of force component required to expand the host casing:

1. Full contact between expandable and host casings.
2. No friction between expandable and host casings.

The free body diagram showing forces on elements of host and expandable casing is described in Appendix.

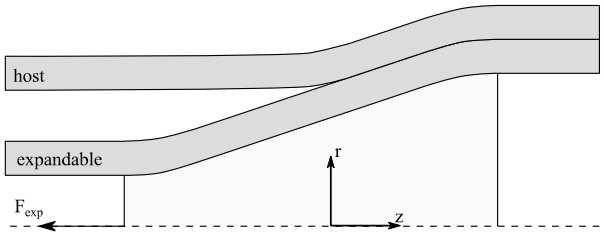

Fig. 6 Deformation of expandable and host casings in overlap expansion

III. Experimental Setup

Small-scale experiments are performed on overlap expansion where host casings with different wall thicknesses are used to generate different pressure on the outer surface of the expandable casing during expansion. The objective of the experiment is to analyze the influence of the external pressure on the axial strain of the expandable casing during expansion.

An expandable casing 2 3/8" S355J2H is expanded with a cone against a P110 host casing which is machined to the desired thickness. The expansion ratio of the expandable casing is about 17 %. Both casings are welded to a flange and expanded in tension as illustrated in Fig. 7. A lubricant is applied between expandable casing and cone. A Linear Variable Differential Transformer (LVDT) is installed to measure the axial displacement of expandable casing relative to the host casing. The axial displacement of the host casing is measured at different time instants during expansion. The experiment is performed in three series where in each series different casing thickness are used as illustrated in Table I. Then, a microscopic inspection is performed on the inner surface of the expandable casing selected from the case with host casing thickness of 11 mm from Series-2. The inspection is repeated for expandable casing expanded freely.

TABLE I
Host casing thicknesses in series

Series-1 [mm]	Series-2 [mm]	Series-3 [mm]
8	8	10.5
11	9.5	
12	11	

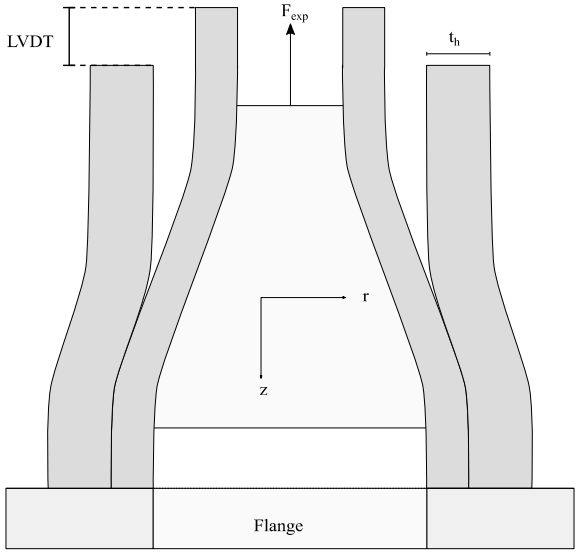

Fig. 7 Schematic of the small-scale overlap expansion

IV. Results

A. Physical Modelling

Multiple FE simulations have been performed on overlap expansion. Both expansion forces and amount of shortening of casing have been calculated in these simulations. Two cases are considered: (1) an expandable casing is expanded against an unexpanded host casing, (2) an expandable casing is expanded against an expanded host casing. The casings are tabulated in Table II. The results from FE simulations and physical model for expansion forces and axial strain are plotted in Figs. 8 and 9.

TABLE II
Casings Considered in Analysis

Casing	Material	OD [inch]	Thickness [inch]	Cone size [inch]
Expandable	VM50	9.625	0.435	
Host	VM50	9.625	0.435	10.2
Host	P110	11.75	0.534	

The results show a good agreement in expansion forces and a significant difference in axial strain. The major difference appears when P110 casing is used. The reason is related to bending of host casing P110 during expansion which results in a smaller contact area. Thus, an increase in contact pressure appears which leads to more axial strain.

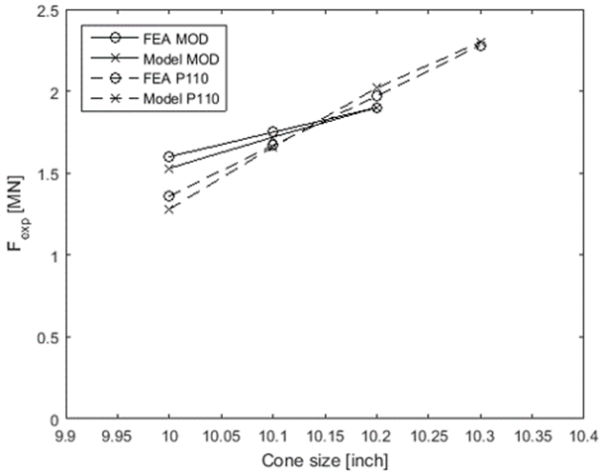

Fig. 8 Comparison between forces calculated through FE simulations and physical model

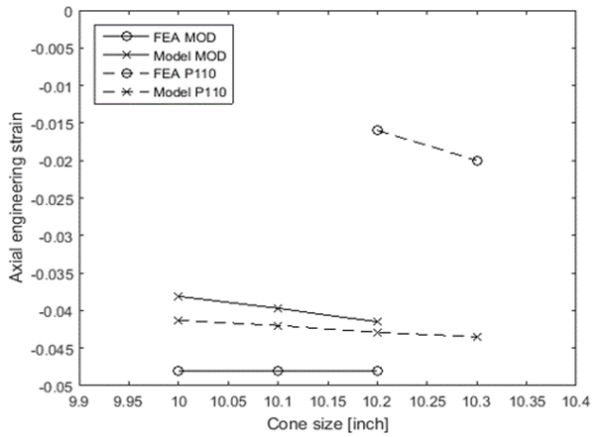

Fig. 9 Comparison between axial strain calculated through FE simulations and physical model

B. Small Scale Experiments

The axial strains and expansion forces measured in the experiment and calculated by the physical model are plotted in Figs. 10 and 11 respectively. Fig. 10 shows the occurrence of ironing at high external pressure and axial strain becomes nonlinear after a certain limit. Analyses with the physical model are performed with different friction factor between cone and expandable casing at different host casing wall thicknesses and results such as axial strain and expansion forces are added to Figs. 10 and 11 respectively. The results show that expansion force increases linearly as the pressure exerted by the host casing increases even at different friction factor as illustrated in Fig. 11. However, the axial strain becomes nonlinear at high contact pressure and high friction factor as shown in Fig. 10. This can be related to the decrease in contact area which leads to increase in contact pressure and subsequently to elongation of casing.

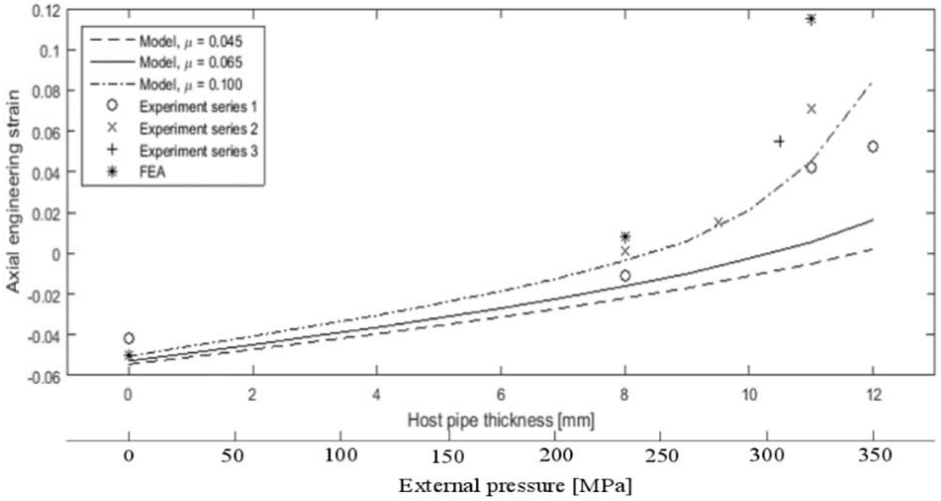

Fig. 10 Comparison in axial strain between experiment and physical model

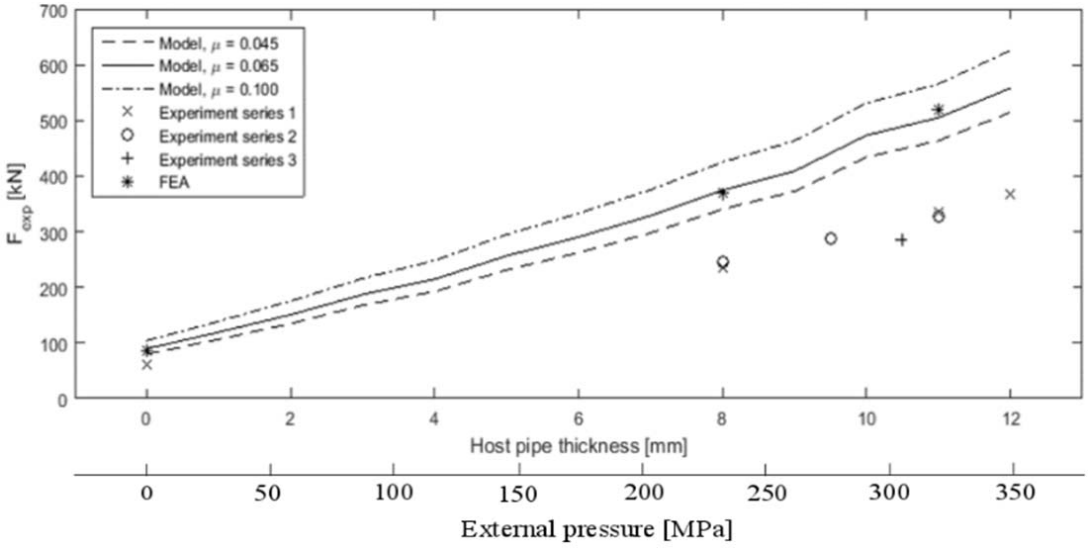

Fig. 11 Comparison in expansion force between experiment and physical model

C. Surface Quality Investigation

The images from microscopic inspection are depicted in Fig. 12. The white areas are representing the areas with maximum height and flattened. The total white area in image of overlap expansion and an image of free expansion are about 20% and 5% of the full scanned area respectively. Therefore, the contact area of the overlap expansion is 4 times the contact area of the free expansion. If the average contact pressure along the cone profile is evaluated for the overlap expansion and free expansion using the physical model, the resulted value of the overlap expansion is also higher than the resulted value of the free expansion by factor 4. This confirms that the increase in external pressure leads to an increase in contact area between the cone and expandable casing. An additional

surface inspection is performed by Atomic Force Microscope (AFM) for the two samples. The inspection shows that the white areas are still covered with the lubricant which means that there is no metal-to metal contact and the friction factor remains the same.

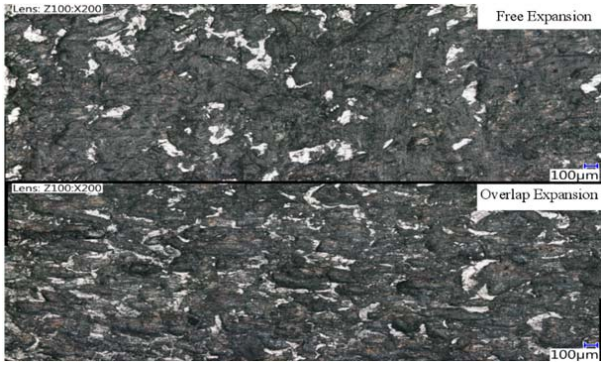

Fig. 12 Microscopic images for free expansion and overlap expansion with 11 mm host casing thickness

V. Conclusion

A model has been developed to calculate the force required to expand a casing during free and overlap expansion, and casing dimensions at post expansion. Results show that expansion forces and axial strains increase with increasing pressure. It is confirmed that when pressures at the outer surface of the casing during expansion exceed a certain limit, ironing occurs. This phenomenon has been confirmed by lab experiments and FE simulations.

The developed model shows good agreement with FE simulations, which are based on the same input parameters. However, there is a difference between measured and predicted expansion forces. For example, the expansion forces for VM50 and S355 casings are generally underestimated by 20% and 35% respectively. One hypothesis on this discrepancy is the difference in contact area between casing and cone as a function of contact pressure, while in the model and FE simulations the contact area is assumed constant. Microscopic inspection shows that contact area increases with increasing pressure, contact pressures are not uniformly distributed on the full contact area and the surface of the expanded casing remains lubricated at high pressures. Other differences might be due to a simplified friction model where the friction coefficient is assumed constant or material model where isotropic hardening is used. The expansion force with respect to contact pressures increases linearly, whereas the axial strain increases exponentially. This strain behavior is due to the nonlinear character of the Von Mises yield surface. This means that the expansion force is quite easy to estimate. However, the strain behavior becomes less predictable at high contact pressures as the parameter sensitivity increases exponentially. For example, small changes in friction coefficient might have a small impact on free expansion, but an enormous impact on overlap expansion.

For future deployments, the difficulty in releasing the LTA due to ironing is mitigated by modifying the design of LTA. Since the LTA can be released now, the ironing in expandable casing with contact between expandable casing and the LTA leads compressive stresses in the unexpanded section of the casing. Severe implications such as buckling of the casing or cone getting stuck may appear and they must be avoided.

Appendix

A. Free Expansion

Since bending occurs at the cone nose, the principle stresses of an element in the casing are not aligned with the global coordinate system. That is, the directions of the stresses follow the cone profile. This means that halfway expansion, the principle stresses can be defined under a certain angle.

It is most convenient to use the stresses and strains in the principle direction to perform an accurate calculation of the plastic behavior of the material. The principle stresses will be referred to as the hoop (circumferential), thickness (radial) and meridional stress and will be written as σ_θ, σ_r and σ_m respectively.

An overview of the pressures and forces acting on a small element in the casing during expansion can be seen in Fig. 5. The fiber lengths at middle, inner and outer surfaces of the casing during bending at cone nose are calculated through:

$$dl_0 = (R_{nose} - 0.5t)d\alpha \quad (1)$$

$$dl_1 = R_{nose}d\alpha \quad (2)$$

$$dl_2 = (R_{nose} - t)d\alpha \quad (3)$$

where R_{nose} and $d\alpha$ are the radius at cone nose and incremental inclination angle.

The fiber lengths at middle, inner and outer surfaces of the casing during bending at cone round off is calculated through:

$$dl_0 = \left(R_{roff} + 0.5t\right)d\alpha \quad (4)$$

$$dl_1 = R_{roff}d\alpha \quad (5)$$

$$dl_2 = (R_{roff} + t)d\alpha \quad (6)$$

where R_{roff} is radius at cone roundoff.

Starting with calculation of force required to increase the diameter of the casing, the forces acting on the cone as shown in Fig. 5 are projected along the z-direction. Since it is assumed that cone moves with a constant speed, Newton's first law is applied and equilibrium equation in z-direction is written as:

$$(N + dN)\cos(\alpha + d\alpha) - N\cos(\alpha) - 2\pi\left(r + \tfrac{1}{2}dr\right)dl_1\mu P_1\cos\left(\alpha + \tfrac{1}{2}d\alpha\right) - 2\pi\left(r + \tfrac{1}{2}dr\right)dl_1P_1\sin\left(\alpha + \tfrac{1}{2}d\alpha\right) + 2\pi\left(r + \tfrac{1}{2}dr + t\cos(\alpha) + \tfrac{1}{2}dt\cos(\alpha)\right)dl_2P_2\sin\left(\alpha + \tfrac{1}{2}d\alpha\right) = 0 \quad (7)$$

After using trigonometric relations for the summation of two angles and assuming an angle increment $d\alpha$, the equilibrium equation in z-direction becomes:

$$(N+dN)(\cos(\alpha)-\sin(\alpha)\,d\alpha)-N\cos(\alpha)-2\pi\left(r+\tfrac{1}{2}dr\right)dl_1\mu P_1\left(\cos(\alpha)-\tfrac{1}{2}\sin(\alpha)\,d\alpha\right)-2\pi\left(r+\tfrac{1}{2}dr\right)dl_1P_1\left(\sin(\alpha)+\tfrac{1}{2}d\alpha\cos(\alpha)\right)+2\pi\left(r+\tfrac{1}{2}dr+t\cos(\alpha)+\tfrac{1}{2}dt\cos(\alpha)\right)dl_2P_2\left(\sin(\alpha)+\tfrac{1}{2}d\alpha\cos(\alpha)\right)=0 \quad (8)$$

Rewriting and neglecting the higher order terms:

$$(dN)\cos(\alpha)-N\sin(\alpha)d\alpha-2\pi r dl_1\mu P_1\cos(\alpha)-2\pi r dl_1P_1\sin(\alpha)+2\pi(r+t\cos(\alpha))dl_2P_2\sin(\alpha)=0 \quad (9)$$

Simplifying after dividing by *cos(α)*:

$$dN-N\tan(\alpha)d\alpha-2\pi r dl_1\mu P_1-2\pi r dl_1P_1\tan(\alpha)+2\pi(r\tan(\alpha)+t\sin(\alpha))dl_2P_2=0 \quad (10)$$

Considering a thin walled pressure vessel, the normal forces are:

$$N=2\pi\sigma_m tr \quad (11)$$

$$N+dN=2\pi(\sigma_m+d\sigma_m)(t+dt)(r+dr) \quad (12)$$

Subtracting both equations, the normal force increment is determined:

$$dN=2\pi(\sigma_m r dt+r t d\sigma_m+\sigma_m t dr) \quad (13)$$

After substituting the determined *N* and *dN* into the equilibrium equation:

$$r\sigma_m dt+r t d\sigma_m+\sigma_m t dr-rt\sigma_m\tan(\alpha)\,d\alpha-r dl_1\mu P_1-r dl_1P_1\tan(\alpha)+(r+t\cos(\alpha))dl_2P_2\tan(\alpha)=0 \quad (14)$$

After dividing by tdl_1, the differential equation in z-direction is determined:

$$\frac{r}{t}\sigma_m\frac{dt}{dl_1}+\frac{d(r\sigma_m)}{dl_1}-r\sigma_m\tan(\alpha)\frac{d\alpha}{dl_1}-\frac{r}{t}\mu P_1-\frac{r}{t}P_1\tan(\alpha)+\left(\frac{r}{t}+\cos(\alpha)\right)\frac{dl_2}{dl_1}P_2\tan(\alpha)=0 \quad (15)$$

The forces on cone are projected along the radial direction. Applying Newton's first law, the equilibrium equation in r-direction:

$$\pi P_{r1}\left(r+\tfrac{1}{2}dr\right)dl_1\cos\left(\alpha+\tfrac{1}{2}d\alpha\right)-\pi P_{r2}\left(r+\tfrac{dr}{2}+t\cos(\alpha)+\tfrac{1}{2}dt\cos(\alpha)\right)dl_2\cos\left(\alpha+\tfrac{1}{2}d\alpha\right)-2\sigma_\theta\left(t+\tfrac{1}{2}dt\right)dl_0\cos\left(\alpha+\tfrac{1}{2}d\alpha\right)-N\sin(\alpha)+(N+dN)\sin(\alpha+d\alpha)=0 \quad (16)$$

After applying trigonometric relations for addition of two angles and neglecting higher order terms, the equation becomes:

$$\pi P_{r1}r dl_1\cos(\alpha)-\pi P_{r2}(r dl_2+t\cos(\alpha)dl_2)\cos(\alpha)-2\sigma_\theta t dl_0\cos(\alpha)+N\cos(\alpha)d\alpha+dN\sin(\alpha)=0 \quad (17)$$

After substituting *N* and *dN* in equilibrium equation in r-direction and simplifying, the equation becomes:

$$\sigma_\theta=\frac{\pi P_{r1}}{2}\frac{r dl_1}{t dl_0}-\frac{\pi P_{r2}}{2}\frac{dl_2}{dl_0}\left(\frac{r}{t}+\cos(\alpha)\right)+\left(\frac{\pi\sigma_m r d\alpha}{dl_0}+\frac{\pi\sigma_m r\tan(\alpha)}{t}\frac{dt}{dl_0}+\right)+\frac{\pi\tan(\alpha)d(r\sigma_m)}{dl_0} \quad (18)$$

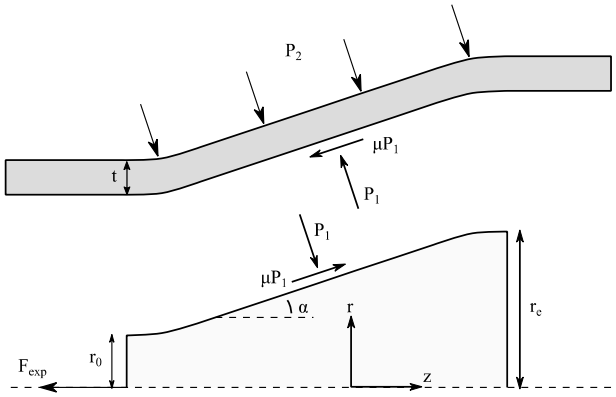

Fig. 13 Free body diagram

The free body diagram in Fig. 4 shows the pressure applied on the cone surface. The pressure components in radial direction are calculated from the pressure applied on the cone surface through:

$$P_{r1}=P_1(\cos(\alpha)-\mu\sin(\alpha)) \quad (19)$$

$$P_{r2}=P_2\cos(\alpha) \quad (20)$$

The expansion force is determined according to the free body diagram depicted in Fig. 4:

$$F_{exp}=\int_0^{2\pi}\int_{r_0}^{r_e}P_1(1+\mu cot(\alpha))r dr d\theta \quad (21)$$

If inner and outer pressures have linear influence on the radial stress in the middle of the pipe, the radial stress is determined by:

$$\sigma_r=-\frac{P_1+P_2}{2} \quad (22)$$

Using Lévy-Mises stress-strain relation during plastic deformation [8], the relation between equivalent plastic strains and deviatoric stresses are stated:

$$\frac{d\varepsilon_\theta}{\sigma'_\theta}=\frac{d\varepsilon_r}{\sigma'_r}=\frac{d\varepsilon_m}{\sigma'_m} \quad (23)$$

The deviatoric stresses σ'_θ, σ'_r and σ'_m are determined by the following relations:

$$\sigma'_\theta=\sigma_\theta-\sigma_{hyd} \quad (24)$$

$$\sigma'_r=\sigma_r-\sigma_{hyd} \quad (25)$$

$$\sigma'_m=\sigma_m-\sigma_{hyd} \quad (26)$$

$$\sigma_{hyd}=\frac{1}{3}(\sigma_\theta+\sigma_r+\sigma_m) \quad (27)$$

The strains are determined through the following relations:

$$d\varepsilon_\theta = \ln(\frac{r+dr}{r}) \quad (28)$$

$$d\varepsilon_t = d\varepsilon_\theta \frac{\sigma'_\theta}{\sigma'_t} \quad (29)$$

Due to material incompressibility during plastic deformation, the strain increment in the meridional direction is determined by:

$$d\varepsilon_m = -d\varepsilon_\theta - d\varepsilon_t \quad (30)$$

Casing bending causes additional strain in the form of elongation and shortening at the inside and outside fibers of the material. The location of the tensile and compressive strains depends whether the bending moment is applied inward or outward. The additional strains have an impact on the expansion force. To take this effect into account, the effective strain is defined as a superposition of two effective strains:

$$d\varepsilon_e = d\varepsilon_{exp} + d\varepsilon_{bend} \quad (31)$$

The initial fiber lengths at the middle, inside and outside the casing are known. An additional strain due to bending can be added. Let dl_n, dl_1 and dl_2 be the fiber length at the neutral axis, inner surface and outer surface respectively. Then the strains at inside and outside of the casing are determined respectively by:

$$\varepsilon_{m,i} = \ln(\frac{dl_1}{dl_n}) \quad (32)$$

$$\varepsilon_{m,o} = \ln(\frac{dl_2}{dl_n}) \quad (33)$$

The strain increments are determined by:

$$d\varepsilon_{m,i} = \varepsilon_{m,i}^s - \varepsilon_{m,i}^{s-1} \quad (34)$$

$$d\varepsilon_{m,o} = \varepsilon_{m,o}^s - \varepsilon_{m,o}^{s-1} \quad (35)$$

where *s* and *(s-1)* are the current and previous time steps.

Calculation of the bending strains requires the knowledge of the fiber length at the neutral axis and its location with respect to the casing thickness. For example, in pure bending the neutral axis lies in the middle of the casing thickness. However, when the material is exposed to additional tensional forces, the neutral axis moves such that the tensional strains during bending are dominant as illustrated in Fig. 5 where t_n is the distance between the inner fiber of the casing and the neutral axis.

Assuming a linear distribution of the axial strain across the thickness, the average axial strain due to bending is:

$$d\varepsilon_{m,bend}^n = \frac{1}{2}\left[\left(1-\frac{t_n}{t}\right)|d\varepsilon_{m,o}| + \frac{t_n}{t}|d\varepsilon_{m,i}|\right] \quad (36)$$

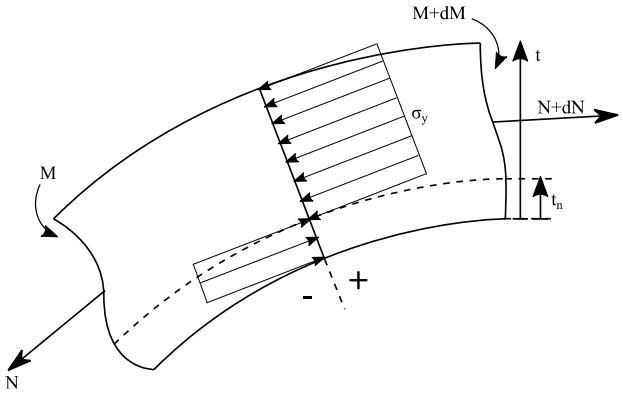

Fig. 14 Stress distribution during plastic deformation

Assuming no change in hoop strain during bending and material is incompressible during plastic deformation, the average strain increment in thickness direction is determined by:

$$d\varepsilon_{t,bend} = -d\varepsilon_{m,bend} \quad (37)$$

The effective strain due to bending is calculated by:

$$d\varepsilon_{e,bend} = \sqrt{\frac{4}{3}d\varepsilon_{m,bend}^2} \quad (38)$$

The normal force at equilibrium during the additional strains due to bending is calculated by:

$$N = \int_{t_n}^{t} 2\pi(r+t)\sigma_e dt - \int_0^{t_n} 2\pi(r+t)\sigma_e dt \quad (39)$$

Calculating the integral in (39) yields:

$$N = 2\pi\sigma_e[r(t-2t_n) + \frac{1}{2}(t^2 - 2t_n^2)] \quad (40)$$

where $\sigma_e = \sigma_y$ at $\varepsilon_0=0$ and $\sigma_e = C(\varepsilon_0)^n$ at $\varepsilon_0>0$ after applying the Ludwik power law [8].

Rearranging (40) gives the following quadratic equation with t_n as an unknown:

$$t_n^2 + 2rt_n + \left[\frac{N}{2\pi\sigma_e} - t\left(r+\frac{1}{2}t\right)\right] = 0 \quad (41)$$

Equation (41) is solved after calculating the force N from the stress in the meridional direction:

$$N = \int_0^t 2\pi(r+t)\sigma_m dt \quad (42)$$

The last stage in the expansion process is bending the casing outward as shown in Fig. 3. Since bending at this stage occurs after increasing the casing inner diameter, this force component is not included in the expansion force calculated previously. Moreover, as the material has to be brought back to its yield stress, this bending force cannot be neglected. The expansion force is updated after calculating the equivalent strain due to this bending $d\varepsilon_{m,bend}$.

The stress strain behavior of the casing is described by

Swift law [8], where the material parameters including C and n values are determined from tensile tests of samples extracted from the casings:

$$\sigma_e = C(\varepsilon_0 + \varepsilon_e)^n \quad (43)$$

B. Overlap Expansion

The expansion of the host casing starts when outer diameter of the expandable casing becomes larger than the inner diameter of the host casing as depicted in Fig. 6.

The pressure required to expand the host casing is applied as an external pressure on the expandable casing. The free body diagram of the overlap expansion is sketched in Fig. 9 and it is used to formulate the expansion force in overlap expansion.

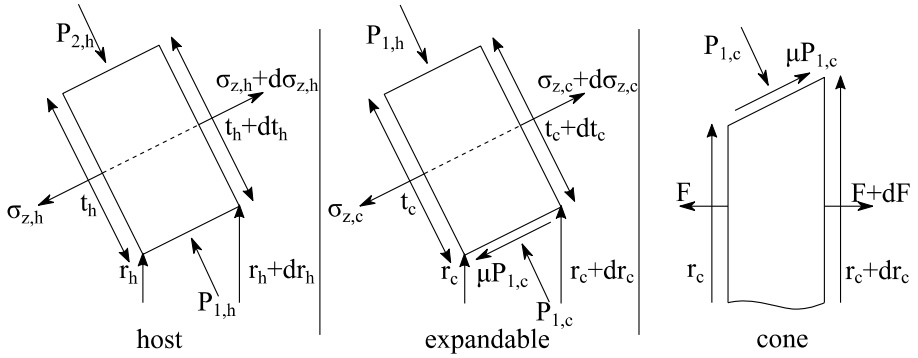

Fig. 15 Free body diagram of overlap expansion

The force components required for bending host casing at the nose and roundoff are determined separately. Since the host casing is thicker than the expandable casing, the force component due to bending becomes significant. The strains due to bending depend on radii of curvature at nose and round off where the host casing is bent. Therefore, the radii must be determined accurately for the expansion force to be calculated accurately.

Like expandable casing, host casing undergoes the same stages of plastic deformation depicted in Fig. 3. The force components are determined in the same manner as in free expansion.

ACKNOWLEDGMENT

The authors would like to thank Djurre Zijsling for his theoretical and experimental support.

REFERENCES

[1] M. Jabs, W. Portas, D. Zijsling, "Expandable technology monodiameter (MoD) achieves milestone," Shell Journal of Technology, 2012.
[2] D. Campo, C. Williams, A. Filippov, L. Cook, D. Brisco, B. Dean, L. Ring, "Monodiameter Drilling Liner - From Concept to Reality," in International Association of Drilling Conference, Amsterdam, 2003.
[3] K. Dupal, D. Campo, C. Andrews, R. Cook, L. Ring, P. York, "Realizationof the Monodiameter Well: Evolution of a Game-Changing Technology," in Offshore Technology Conference, Houston, 2002.
[4] M. F. Shi, J. Gerdeen, "A theoretical study of the ironing process in sheet metal forming," Journal Materials Shaping Technology, vol. 7, pp. 203--211, 1989.
[5] L. Baillet, M. Brunet, Y. Berthier, "Experimental and numerical dynamic modelling of ironing process," Journal of Materials Processing Technology, vol. 60, pp. 677--684, 1996.
[6] D. Chang, J. Wang, "Influence of process parameters on the ironing of deep-drawn cups," Journal of Manufacturing Science and Engineering, vol. 119, pp. 699--705, 1997.
[7] J. Tirosh, D. Iddan, M. Silviano, "Hydrostatic ironing -- Analysis and experiments," Journal of Engineering for Industry, vol. 114, pp. 237--243, 1992.
[8] J. Chakrabarty, Theory of Plasticity, McGraw-Hill, 2006.